Research Square

Preprints are preliminary reports that have not undergone peer review.
They should not be considered conclusive, used to inform clinical practice,
or referenced by the media as validated information.

Evaluation of image quality at the detector's edge of dedicated breast positron emission tomography

Yoko Satoh (ysatoh@ypic.jp)
Yamanashi PET imaging clinic https://orcid.org/0000-0002-0188-0906
Utaroh Motosugi
Department of Radiology, Kofu-kyoritsu hospital
Masamichi Imai
Saint Thomas' Hospital
Yoshie Omiya
Yamanashi Daigaku Igakubu Daigakuin Sogo Kenkyubu Igakuiki
Hiroshi Onishi
Yamanashi University

Original research

Keywords: dedicated breast positron emission tomography, 18F-fluorodeoxyglucose, image quality, edge of detector

Posted Date: July 25th, 2020

DOI: https://doi.org/10.21203/rs.3.rs-21524/v2

License: This work is licensed under a Creative Commons Attribution 4.0 International License.
Read Full License

Version of Record: A version of this preprint was published on January 18th, 2021. See the published version at https://doi.org/10.1186/s40658-020-00351-6.

Abstract

Background: We assessed image quality of dedicated breast positron emission tomography (dbPET) at the detector's edge by phantom and clinical studies.

Methods: A breast phantom with four spheres (16, 10, 7.5, and 5 mm diameter) was filled with ^{18}F-fluorodeoxyglucose solution (sphere-to-background ratio, 8:1). The spheres occupied five different positions from the top edge to the centre of the detector and were scanned for 5 min in each position. Reconstructed images were visually evaluated, and % background variability ($\%N_{5mm}$), % contrast ($\%Q_{H,5mm}$), and contrast-to-noise ratio ($Q_{H,5mm}/N_{5mm}$) for the 5 mm sphere; and coefficient of variation of the background ($CV_{background}$) were calculated. Subsequently, clinical cases were analysed. Tumour-to-background ratios (TBRs) between breast cancer near the chest wall (close to the detector's edge; peripheral group) and at other locations (non-peripheral group) were compared. The TBR of each lesion was compared between dbPET and PET/computed tomography (CT).

Results: Closer to the detector's edge, the $\%N_{5mm}$ and $CV_{background}$ increased and $\%Q_{H,5mm}$ and $Q_{H,5mm}/N_{5mm}$ decreased in the phantom study. The disadvantages of this placement were visually confirmed. Regarding clinical images, TBR of dbPET was significantly higher than that of PET/CT in both the peripheral (12.1±6.2 vs. 6.5±3.4, p=0.0001) and non-peripheral (13.1±7.1 vs. 7.7±7.4, p=0.0004) groups. There was no significant difference in TBR of dbPET between the peripheral and non-peripheral groups (12.1±6.2 vs. 13.1±7.1, p=0.6367).

Conclusion: The phantom study revealed poorer image quality closer to the detector edge at a depth of 1/8 of the axial field of view (FOV) than at other more central parts. In clinical studies, however, lesion detectability of dbPET was the same regardless of the lesion position, and it was higher than that in PET/CT. dbPET has a great potential for detecting breast lesions near the chest wall if they are within the FOV, even in young women with small breasts.

Background

^{18}F-fluorodeoxyglucose (FDG) positron emission tomography/computed tomography (PET/CT) has become one of the most useful tools in diagnostic imaging for cancer. Many studies have demonstrated the efficacy of whole-body FDG-PET/CT in staging or re-staging, in monitoring the response to therapy, and for predicting the prognosis of patients with breast cancer [1-3]. It is important to detect breast cancer at an early stage when the lesions are small, since mortality increases with tumours exceeding 1 cm in size [4,5]. However, detection of small breast cancers by whole-body PET/CT is challenging because of its limited spatial resolution [6]. High-resolution dedicated breast PET (dbPET) scanners have been developed to detect small breast lesions. There are two types of high-resolution dbPET, i.e. positron emission mammography (PEM) and a tomographic technique using a ring-shaped scanner (ring-shaped dbPET) [7]. PEM systems depict breast tissue via soft compression of the breast with two opposing plate-like detectors and have higher sensitivity for detecting small lesions than whole-body PET/CT [8-10].

Ring-shaped dbPET scanners can visualise breast cancer more clearly than whole-body PET/CT [11,12]. These high-resolution breast PET systems have greater photon sensitivity and can improve spatial resolution by setting the detector close to the breast, reducing respiratory movement (either by fixing the breast to the PEM detector or by scanning in the prone position for dbPET), and using smaller detection units than those of whole-body PET/CT. Their performances have been evaluated using NEMA-NU4-2008 standards [13], and the physical parameters of dbPET and whole-body PET/CT have been compared using a common breast phantom [14]. In that comparative study, the breast phantom was located at the centre of each scanner, and no studies have reported on the quality of dbPET images close to the edge of the detector. However, many Japanese women have small breasts, and their mammary glands are often located near the chest wall, close to the edge of detector, even when they are in the prone position. This tendency is particularly common in young women who are less likely to have breast ptosis than older women. Therefore, it is necessary to evaluate the consequences of a shift in the position of the breast phantom away from the centre of the detector. This study aimed to confirm the image quality of dbPET at the edge of the detector by phantom and clinical studies.

Methods

This single-institution study was approved by the institutional review board and ethics committee of our institute in accordance with the Declaration of Helsinki; written informed consent was obtained from each patient for access to their data.

Ring-shaped dbPET scanner

The ring-shaped dbPET scanner (Elmammo, Shimadzu Corp., Kyoto, Japan) consists of 36 detector modules arranged in three contiguous rings, has a diameter of 195 mm and an axial length of 156.5 mm, and has depth-of-interaction measurement capability [15]. The transaxial effective field-of-view (FOV) is 185 mm. Each detector block consists of a four-layered 32 × 32 array of lutetium oxyorthosilicate crystals coupled to a 64-channel positron-sensitive photomultiplier tube via a light guide. Attenuation correction was calculated using a uniform attenuation map with object boundaries obtained from emission data [16]. Scatter correction was performed using the convolution-subtraction method [17] with kernels obtained by background tail fitting. The characteristics and standard performance of this scanner have been reported in detail previously [13].

Whole-body PET/CT scanner

PET/CT scans were obtained using a Biograph Horizon TrueV FDG-PET/CT system (Siemens Medical Solutions, Knoxville, TN, USA). This system has 52 detector rings consisting of 160 blocks, with each block containing an array of 13 × 13 lutetium oxyorthosilicate crystals (4 mm × 4 mm × 20 mm) covering an axial FOV of 221 mm and a transaxial FOV of 690 mm. A CT scan was performed for attenuation correction (130 kV; 15–70 mA; tube rotation time, 0.6 s per rotation; pitch, 1; a transaxial FOV, 700 mm; and section thickness, 5 mm).

Development and preparation of the breast phantom

A cylindrical breast phantom containing four plastic spheres of different diameters was used. The inner and outer diameters of the cylinder were 100 mm and 140 mm, respectively, and the height was 170 mm. The diameters of the spheres arranged inside were 5, 7.5, 10, and 16 mm. Spheres smaller than 5 mm in diameter were not used because they could not be detected by PET/CT. Therefore, the detectability of lesions smaller than 5 mm was not evaluated in this study. The cylinder and four spheres were filled with ^{18}F-FDG solution at a sphere-to-background radioactivity ratio of 8:1 in accordance with a previous study [14]. The background radioactivity at the start of data acquisition by dbPET was set to 2.46 kBq/mL. One scan was performed under each condition.

Data acquisition and image reconstruction

The breast phantom was positioned such that the spheres were precisely located in the same axial plane at different positions in the axial field of view. The spheres were positioned at 8 mm, 13 mm, 19.5 mm (1/8 of axial FOV), 39 mm (1/4 of axial FOV), and 78 mm (1/2 or halfway point of the axial FOV) below the top edge of the detector (Figure 1). Since it is unlikely that a breast lesion is located at the bottom edge of the detector, only the chest wall side of the detector was evaluated. Sphere placement at each position in the detector was confirmed visually and by measurement on the image. The dbPET images were reconstructed using a three-dimensional list mode dynamic row-action maximum-likelihood algorithm with one iteration and 128 subsets, a relaxation control parameter of β=20, and a matrix size in the axial view of 236 × 200 × 236 with a post-reconstruction smoothing Gaussian filter (1.17-mm FWHM). Tight or just mode attenuation correction using a uniform attenuation map with object boundaries obtained from the emission data was performed on phantom or clinical dbPET images, respectively. The scatter correction method used was the convolution-subtraction method with kernels obtained by background tail-fitting [17].

The clinical PET/CT images were reconstructed using the ordered subset expectation maximisation method and the time-of-flight (TOF) algorithm with four iterations and 10 subsets. The CT data were resized from a 512 × 512 matrix to a 180 × 180 matrix to match the PET data and construct CT-based transmission maps for attenuation correction of the PET data with a post-reconstruction smoothing Gaussian filter (5 mm FWHM).

Analyses of phantom image quality

Visual analyses of the phantom images were performed using syngo.via VB10 (Siemens Healthcare GmbH, Erlangen, Germany). An experienced nuclear medicine physician and two experienced PET technologists evaluated the hot spheres. Evaluations were performed using the slices displayed in the transverse image slice containing the sphere centres. The images were displayed in an inverse grey scale with a standardised uptake range of 0–6. The 5-mm-diameter hot sphere was visually graded as follows: 2, identifiable; 1, visualised, but similar hot spots observed elsewhere; and 0, not visualised. Spheres with visual scores ≥1.5 were deemed to be detectable. The final score was the mean of the scores from three

readers. The visual assessment was performed based on the Japanese guidelines [18]. Physical analysis was also performed using syngo.via VB10. The coefficient of variation of the background ($CV_{\text{background}}$), % background variability ($\%N_{5\text{mm}}$), % contrast ($\%Q_{H,5\text{mm}}$), and contrast-to-noise ratio ($Q_{H,5\text{mm}}/N_{5\text{mm}}$) were calculated. The $CV_{background}$ was calculated by evaluation of various regions of interest (ROIs) in the transverse image slice that contained the sphere centres. Ten ROIs with a diameter of 16 mm were placed in the background region in that slice and ±5-mm–adjacent slices (30 ROIs in total).

See formula 1 in the supplementary files.

$\%Q_{\text{H},5\text{mm}}$, $\%N_{5\text{mm}}$, and their ratio ($\%Q_{\text{H},5\text{mm}}/N_{5\text{mm}}$) were also calculated by evaluation of various ROIs. The 12 ROIs that were 5 mm in diameter were placed on the background region in that slice and ±5-mm–adjacent slices (36 ROIs in total). $\%Q_{\text{H},5\text{mm}}$ and $\%N_{5\text{mm}}$ were used as measures for the image contrast and noise for the sphere, and their ideal values were 100% and 0%, respectively.

See formula 2 and 3 in the supplementary files.

These physical values were calculated according to a previous report [19].

Analysis of human images

Of a total of 202 consecutive women who underwent both dbPET and whole-body PET/CT scans from August 2016 to September 2019, 62 histologically proven breast cancer tumours of 57 women with positive findings on both dbPET and whole-body PET/CT images were included in the study. Patients fasted at least 6 hours prior to administration of ^{18}F-FDG (3 MBq/kg) and were scanned by whole-body PET/CT for 90 s per bed and dbPET for 7 min per breast. Scans were performed at 60- and 90-min post-injection, both in the prone position. The PET/CT and dbPET images were reconstructed using the same conditions as for the phantom images.

All PET images were evaluated separately by two experienced nuclear medicine physicians (with 16 and 7 years of experience in interpreting PET, respectively). Of the 62 lesions, those in which the shortest distance from the detector edge on the chest wall side to the tumour centre was 2 cm or less on the axial image of dbPET were defined as the “peripheral group”; the other lesions were defined as the “non-peripheral group”. Non-mass uptakes, other than focus and mass-like uptakes, were excluded because their quantitative reliability could not be established.

Tumours that were exactly centred in both peripheral and non-peripheral regions and whose volume was equally present in both regions were also excluded.

The quantitative value of PET is known to be affected by the partial volume effect [20]. To account for lesion size bias, propensity matching was performed to compare the peripheral and non-peripheral groups. The non-peripheral group was reorganised such that lesion size matched the peripheral group in

a one-to-one correspondence. As a result, 23 lesions in each group (total 46 lesions) were included in the final analysis.

To evaluate lesion detectability in dbPET depending on the position of the tumour, tumour-to-background ratio (TBR) was calculated as follows. First, the smallest spheroid volume of interest (VOI) that just contained the tumour was placed on the monitor. Second, 5-mm-diameter spherical VOIs were placed at 6 locations on the top, bottom, left, right, anterior, and posterior of the tumour, as close as possible to it, in the non-peripheral group. Five VOIs were used in the peripheral group; the posterior VOI was excluded because there was not enough space to place it posterior of the tumour (Figure 2). The TBR was the maximum standardised uptake value (SUV_{max}) of the VOI on the tumour divided by an average SUV_{mean} of the five (6) VOIs on the background. The TBRs were compared between dbPET and PET/CT images, and the TBR of dbPET was compared between the peripheral and non-peripheral groups. Additionally, the SUV_{max} and the SUV_{peak} (maximum average SUV within a 1-cm^3 spherical volume) were measured and compared between groups and between devices.

Statistical analysis

A paired t-test was used to compare the TBR of dbPET and whole-body PET/CT for the peripheral and non-peripheral groups, respectively. The Mann–Whitney U test was used to test for differences in TBR on dbPET between peripheral and non-peripheral lesion groups. The correlations between SUV_{max} and SUV_{peak} on dbPET and on WB-PET/CT were evaluated using Pearson correlation coefficients. Statistical significance was defined as $p<0.05$. Additionally, for these PET measurements, interclass correlation coefficients (ICC) were used to evaluate the reliability between readers.

Results

dbPET phantom studies

Images of the breast phantom scanned by dbPET at the five different positions are shown in Figure 3. In the qualitative evaluation, the visual scores recorded by a nuclear medicine physician and two nuclear medicine technologists on the dbPET images at 8 mm, 13 mm, 19.5 mm (depth of 1/8), 39 mm (depth of 1/4), and 78 mm (depth of 1/2, the centre of the detector) below the top edge of the detector were 0, 0.33, 1.67, 2, and 2, respectively (Table 1). Second, in the quantitative evaluations, the $\%N_{5mm}$, $\%Q_{H,5mm}$, $Q_{H,5mm}/N_{5mm}$, and $CV_{background}$ at the centre of the detector were 6.41, 10.02, 1.56, and 5.91, respectively (Table 1, Figure 4A). The $\%N_{5mm}$ and $CV_{background}$ increased and $\%Q_{H,5mm}$ and $Q_{H,5mm}/N_{5mm}$ decreased when the phantom was placed closer to the edge of the detector (Table 1, Figure 4B). Image degradation closer to the edge of the detector was confirmed by visual scoring. Based on the results of this phantom study, the boundary line between peripheral and non-peripheral lesions in clinical studies was defined as 2 cm from the upper edge of the detector.

Patient studies

A total of 46 lesions (23 in each group) in 45 breasts of 44 patients (age range: 37–87 y, mean: 57.8 y) were evaluated. One patient had one peripheral and one non-peripheral lesion on one side of her breast, one patient had two peripheral lesions on one side of the breast, and each of the 42 patients had one lesion.

After propensity size matching, the mean diameters of the lesions in the peripheral and non-peripheral groups were 19.3±12 mm and 20±12.2 mm (p=0.7663), respectively (Table 2). The ICC of the TBR was excellent (0.92 for PET/CT and 0.89 for dbPET). The values evaluated by one reader with greater experience were analysed in this study. There were strong linear correlations between the SUV_{max} and SUV_{peak} of dbPET and whole-body PET/CT in both the peripheral group ([SUV_{max}; r=0.88, p <0.0001], [SUV_{peak}; r=0.94, p <0.0001]) and non-peripheral group ([SUV_{max}; r=0.88, p<0.0001], [SUV_{peak}; r=0.96, p<0.0001]) (Figure 5). The TBR of dbPET was significantly higher than that of whole-body PET/CT in both the peripheral and non-peripheral groups (p<0.0001, Figure 6A). There was no significant difference in the TBR of dbPET between the peripheral and non-peripheral groups (p=0.6367, Figure 6B). Figure 7 shows representative cases of peripheral and non-peripheral breast cancer acquired by dbPET and PET/CT. The breast cancers were visualised on dbPET more easily than on PET/CT regardless of the location of the lesion (peripheral or non-peripheral).

Discussion

In this study, we evaluated the image quality obtained at different locations within the detector for ring-type breast PET. In the phantom study, the closer to the top of the detector, the higher the $CV_{background}$ and $\%N_{5mm}$, and the lower the $\%Q_{H,5mm}$ and $\%Q_{H,5mm}/N_{5mm}$ were. These results indicated that the quantitative measurements were almost equal except for the end of one-eighth of the detector (about 2 cm from the end of the detector).

Minoura et al. reported that dbPET images show high levels of noise at the edge of the detector (the bottom of the detector or the chest wall side) and showed the relationship between the slice position in the dbPET image and the standard deviation of noise [21]. Our results showing that dbPET image quality decreases at 1/8 of the detector edge are consistent with their reports. The geometric efficiency by Monte Carlo simulation at a detector depth of 1/8 was calculated as 0.2, which is considerably lower than that at the centre, which was 0.65. Usually, whole-body PET scans use overlapping acquisition beds to correct for reduced sensitivity at the detector edges; acquisition of data in overlapped regions can improve quantitative accuracy [22,23]. However, since the dbPET scanner is fixed and cannot use overlapping acquisition to improve image quality near the edges of the detector, there are concerns that important information may be missed. Additionally, out-of-FOV radioactivity, among which myocardial uptake may be most significant, would also significantly affect image quality. The SUV_{max} and SUV_{peak} obtained from dbPET and PET/CT images were highly correlated in this clinical study, regardless of the tumour location, validating these quantitative values of the tumour closer to the edge of dbPET detector. Furthermore, to

better reproduce the same scatter conditions as in real patients, evaluation with a phantom that simulates out-of-FOV radioactivity from the patients' chest is necessary.

Based on the phantom test results, the detectability of clinical dbPET images was compared for lesions located up to 2 cm from the upper edges of the detector and for the other lesions. Contrary to the phantom study results, there was no significant difference in TBR between the two groups. The clinical images had a high TBR in some projection directions, which may have facilitated the detection of lesions. This may be because the phantom image had a uniform background, whereas human breasts have different proportions of mammary glands and fat, and therefore, the physiological of FDG uptake in the background tissue was not uniform. Additionally, the TBR in both groups was significantly higher than that in PET/CT. dbPET has a higher-resolution scanner than conventional whole-body PET/CT, and the prone position significantly supresses respiratory movements compared to whole-body PET/CT scans; therefore, even if the lesion is located at the edge of the detector, dbPET may show higher detectability than PET/CT, which uses overlapping acquisition. Positive and linear correlations were observed between SUV_{max} and SUV_{peak} of PET/CT and dbPET.

dbPET achieves higher sensitivity and resolution than whole-body PET/CT by i) reduction of respiratory movement of the breast by acquisition in the prone position, and ii) bringing the detector close to the breast. The 4-layer depth-of-interaction detector used in dbPET can maintain sensitivity and resolution at the edges of the transverse field of view [24,25]. However, if the background mammary gland shows physiological FDG uptake, the contrast of the lesion and background is higher than that of PET/CT. As a result, the 2018 edition of the Japanese Guidelines for the Practice of Breast Cancer newly describe the use of high-resolution breast PET as a supplemental modality for breasts with high density on mammography, and dbPET is expected to be applied to young women who often have high-density breasts. Both dbPET and PEM have the disadvantage that, due to their structural features, a part of the mammary gland near the chest wall is in the blind area and the lesion may be outside the field of view. However, this study suggests that if the lesion is within the field of view of dbPET, it can be detected with high probability, even at the edge of the detector. Further studies will be needed to clarify the lesions in patients that are likely to be outside the FOV of either dbPET or PEM.

To compare both devices, the clinical participants had to have relatively large lesions that were visually recognizable on both devices. However, given the prognosis of breast cancer, comparison between both systems should focus on smaller lesions. The spatial resolution of whole-body PET/CT has improved due to the development of reconstruction techniques such as TOF and point spread function (PSF) algorithms. In this study, we quantitatively evaluated TOF-reconstructed PET/CT images, since edge artefacts are known to occur in PSF reconstruction and are significant for small lesions [26]. Furthermore, some reports have shown that visualisation of small breast lesions can be improved by performing PET/CT in the prone position using assistive devices to allow breast expansion and suppression of respiratory movements [27, 28]. Reconstruction methods such as PSF and smaller pixel sizes, and scanning in the prone position are expected to improve the visual detection rate of smaller lesions with PET/CT. This will allow a comparison of both devices for smaller lesions.

Our study had several limitations. First, the phantom was scanned only once for each position. The reproducibility of the findings would have been better if the average results of several scans under each condition were calculated. Second, the study design was retrospective, and the patient cohort was small. Because only histologically proven breast cancers were included in this clinical study, small breast cancers near the edge of the detector that are false-negative on PET may not be sufficiently evaluated. It should also be noted that lesions may be difficult to detect with dbPET if the TBR is low due to low FDG uptake in the lesion, or high uptake in the background mammary gland. Studies with larger populations and considerations including histology and subtypes of breast cancer will be required to address these limitations. Third, PET images acquired 90 minutes after injection are known to have improved uptake and contrast compared to those acquired 60 minutes after injection. Because this study was a retrospective study, all patients were scanned 60 and 90 minutes after FDG intravenous injection with PET/CT and dbPET, respectively, under our clinical conditions. This would likely have caused some bias in the results. Randomised prospective studies that appropriately control the start time of the scan are necessary for an accurate comparison of both devices.

Conclusion

In our phantom study, based on the image quality at the depth of 1/8, the quality decreased when the phantom was closer to the edge of the detector. In the clinical studies, however, lesion detectability was the same regardless of whether the lesion was close to the edge of the detector or not, and the detectability in both conditions was higher than that in PET/CT.

Declarations

Funding

This research did not receive any specific grant from funding agencies in the public, or not-for-profit sectors.

Conflicts of Interest

The authors declare that they have no conflict of interest.

Ethics approval and consent to participate

All procedures performed in studies involving human participants were in accordance with the ethical standards of the institutional and/or national research committee (include name of committee + reference number) and with the 1964 Helsinki declaration and its later amendments or comparable ethical standards. This study was approved by the Ethics Committee of Kofu Neurosurgical Hospital and Yamanashi PET imaging clinic. We have obtained informed consent from all the patients included in the study.

Consent for publication: not applicable

Acknowledgement

The authors gratefully acknowledge the assistance of Takao Arai from Yamanashi PET Imaging Clinic in the acquisition of the images.

Availability of data and materials

The datasets used and/or analysed during the current study are available from the corresponding author on reasonable request.

Authors Contribution

All authors contributed to the study design. YS and MI contributed to data collection and analysis. YS wrote the manuscript, and the other authors revised the manuscript. All authors read and approved the final manuscript.

References

1. Groheux D, Espié M, Giacchetti S, Hindié E. Performance of FDG PET/CT in the clinical management of breast cancer. Radiology. 2013;266:388–405.
2. Lee H, Lee DE, Park S, Kim TS, Jung SY, Lee S, et al. Predicting response to neoadjuvant chemotherapy in patients with breast cancer: combined statistical modeling using clinicopathological factors and FDG PET/CT texture parameters. Clin Nucl Med. 2019;44:21–9.
3. Satoh Y, Nambu A, Ichikawa T, Onishi H. Whole-body total lesion glycolysis measured on fluorodeoxyglucose positron emission tomography/computed tomography as a prognostic variable in metastatic breast cancer. BMC Cancer. 2014;14:525.
4. Ichizawa N, Fukutomi T, Iwamoto E, Akashi-Tanaka S. Long-term results of T1a, T1b and T1c invasive breast carcinomas in Japanese women: validation of the UICC T1 subgroup classification. Jpn J Clin Oncol. 2002;32:108–9.
5. Saadatmand S, Bretveld R, Siesling S, Tilanus-Linthorst MM. Influence of tumour stage at breast cancer detection on survival in modern times: population based study in 173,797 patients. BMJ. 2015;351:h4901.
6. Kumar R, Chauhan A, Zhuang H, Chandra P, Schnall M, Alavi A. Clinicopathologic factors associated with false negative FDG-PET in primary breast cancer. Breast Cancer Res Treat. 2006;98:267–74.
7. Bowen SL, Wu Y, Chaudhari AJ, Fu L, Packard NJ, Burkett GW, et al. Initial characterisation of a dedicated breast PET/CT scanner during human imaging. J Nucl Med. 2009;50:1401–8.
8. Kalinyak JE, Berg WA, Schilling K, Madsen KS, Narayanan D, Tartar M. Breast cancer detection using high-resolution breast PET compared to whole-body PET or PET/CT. Eur J Nucl Med Mol Imaging. 2014;41:260–75.

9. Yamamoto Y, Ozawa Y, Kubouchi K, Nakamura S, Nakajima Y, Inoue T. Comparative analysis of imaging sensitivity of positron emission mammography and whole-body PET in relation to tumor size. Clin Nucl Med. 2015;40:21–5.
10. Fowler AM. A molecular approach to breast imaging. J Nucl Med. 2014;55:177–80.
11. Nishimatsu K, Nakamoto Y, Miyake KK. Higher breast cancer conspicuity on dbPET compared to WB-PET/CT. Eur J Radiol. 2017;90:138–45.
12. Nakamoto R, Nakamoto Y, Ishimori T. Diagnostic performance of a novel dedicated breast PET scanner with C-shaped ring detectors. Nucl Med Commun. 2017;38:388–95.
13. Miyake KK, Matsumoto K, Inoue M. Performance Evaluation of a new dedicated breast PET scanner using NEMA NU4-2008 Standards. J Nucl Med. 2014;55:1198–203.
14. Satoh Y, Motosugi U, Imai M, Onishi H. Comparison of dedicated breast positron emission tomography and whole-body positron emission tomography/computed tomography images: a common phantom study. Ann Nucl Med. 2019;34:1–9
15. Qi J, Kuo C, Huesman RH, Klein GJ, Moses WW, Reutter BW. Comparison of rectangular and dual-planar positron emission mammography scanners. IEEE Trans Nucl Sci. 2002;49:2089–96.
16. Yamakawa Y, Kitamura K. Attenuation correction using level set method for application specific PET scanners. IEEE Nucl Sci Symp Conf Rec. 2011;3130–2.
17. Bailey DL, Meikle SR. A convolution-subtraction scatter correction method for 3D PET. Phys Med Biol. 1994;39:411–24.
18. Hosono M, Saga T, Ito K. Clinical practice guideline for dedicated breast PET. Ann Nucl Med. 2014;28:597–602.
19. Fukukita H, Suzuki, K, Matsumoto, K, Terauchi T, Daisaki H, Ikari Y, et al. Japanese guideline for the oncology FDG- PET/CT data acquisition protocol: synopsis of Version 2.0. Ann Nucl Med 2014;28:693–705.
20. Srinivas SM, Dhurairaj T, Basu S, Bural G, Surti S, Alavi A. A recovery coefficient method for partial volume correction of PET images. Ann Nucl Med. 2009;23:341–8.
21. Minoura N, Teramoto A, Ito A, Yamamuro O, Nishio M, Saito K, et al. A complementary scheme for automated detection of high-uptake regions on dedicated breast PET and whole-body PET/CT. Radiol Phys Technol. 2019;12:260–7.
22. Fahey FH. Data acquisition in PET imaging. J Nucl Med Technol. 2002;30:39–49.
23. Panin VY, Smith AM, Hu J, Kehren F, Casey ME. Continuous bed motion on clinical scanner: design, data correction, and reconstruction. Phys Med Biol. 2014;59:6153–74.
24. Yamaya T, Yoshida E, Obi T, Ito H, Yoshikawa K, Murayama H. First human brain imaging by the jPET-D4 prototype with a pre-computed system matrix. IEEE Trans Nucl Sci. 2008;55:2482–92.
25. Akamatsu G, Tashima H, Iwao Y, Wakizaka H, Maeda T, Mohammadi A, et al. Performance evaluation of a whole-body prototype PET scanner with four-layer DOI detectors. Phys Med Biol. 2019;64:095014.

26. 26. Kidera D, Kihara K, Akamatsu G, Mikasa S, Taniguchi T, Tsutsui Y, et al. The edge artifact in the point-spread function-based PET reconstruction at different sphere-to-background ratios of radioactivity. Ann Nucl Med. 2016;30:97–103.
27. 27. Williams JM, Rani SD, Li X, Arlinghaus LR, Lee TC, MacDonald LR, et al. Comparison of prone versus supine 18F-FDG-PET of locally advanced breast cancer: Phantom and preliminary clinical studies. Med Phys. 2015;42:3801–
28. 28. Teixeira SC, Koolen BB, Vogel WV, Wesseling J, Stokkel MP, Vrancken Peeters MJ, et al. Additional prone 18F-FDG PET/CT acquisition to improve the visualization of the primary tumor and regional lymph node metastases in stage II/III breast cancer. Clin Nucl Med. 2016;41:e181–

Tables

TABLE 1. Visual and quantitative assessments of the breast phantom scanned by dbPET at five different positions

Distance[a]	Visual score (average)[b]	$\%Q_{H,5mm}$	$\%N_{5mm}$	$\%Q_{H,5mm}/\%N_{5mm}$	$CV_{background}$
8 mm	0	5.13	11.93	0.43	13.8
13 mm	0.33	6.99	7.63	0.92	12.3
19.5 mm[i)]	1.67	10.92	7.24	1.51	10.2
39 mm[ii)]	2	11.74	7.59	1.55	9.3
78 mm[iii)]	2	10.02	6.41	1.56	5.9

[a] Distance from the upper edges of the detector, i) depth of 1/8, ii) depth of 1/4, iii) depth of 1/2, the centre of the detector. dbPET, dedicated breast positron emission tomography; $\%Q_{H,5mm}$, the percentage of the contrast; $\%N_{5mm}$, the percentage of the background variability; $CV_{background}$, the coefficient of variation of the background. [b] Visual score for the image of the 5-mm-diameter sphere.

TABLE 2. Characteristics of the 46 lesions in 44 patients

Group		Peripheral	Non-peripheral
Number of lesions (women)		23 (22)	23 (23)
Age (median, range)		52 (37–87)	62 (43–79)
Clinical size (mm, median, range)		17 (7–51)	17 (7–52)
Distance from chest wall to lesion (mm, median, range)[a]		0.83 (0.44–1.55)	32.7 (20.2–64.7)
Histopathology	Invasive ductal carcinoma	19	20
	Invasive lobular carcinoma	1	0
	Invasive ductal and lobular carcinoma	1	0
	Other invasive carcinomas	1	0
	Ductal carcinoma in situ	1	3
Subtype	Luminal A/B	9/7	10/5
	HER2 positive	1	2
	Triple negative	2	3
	Unknown	4	3

[a] Distance from the FOV margin on the chest wall to the centre of the lesion

Figures

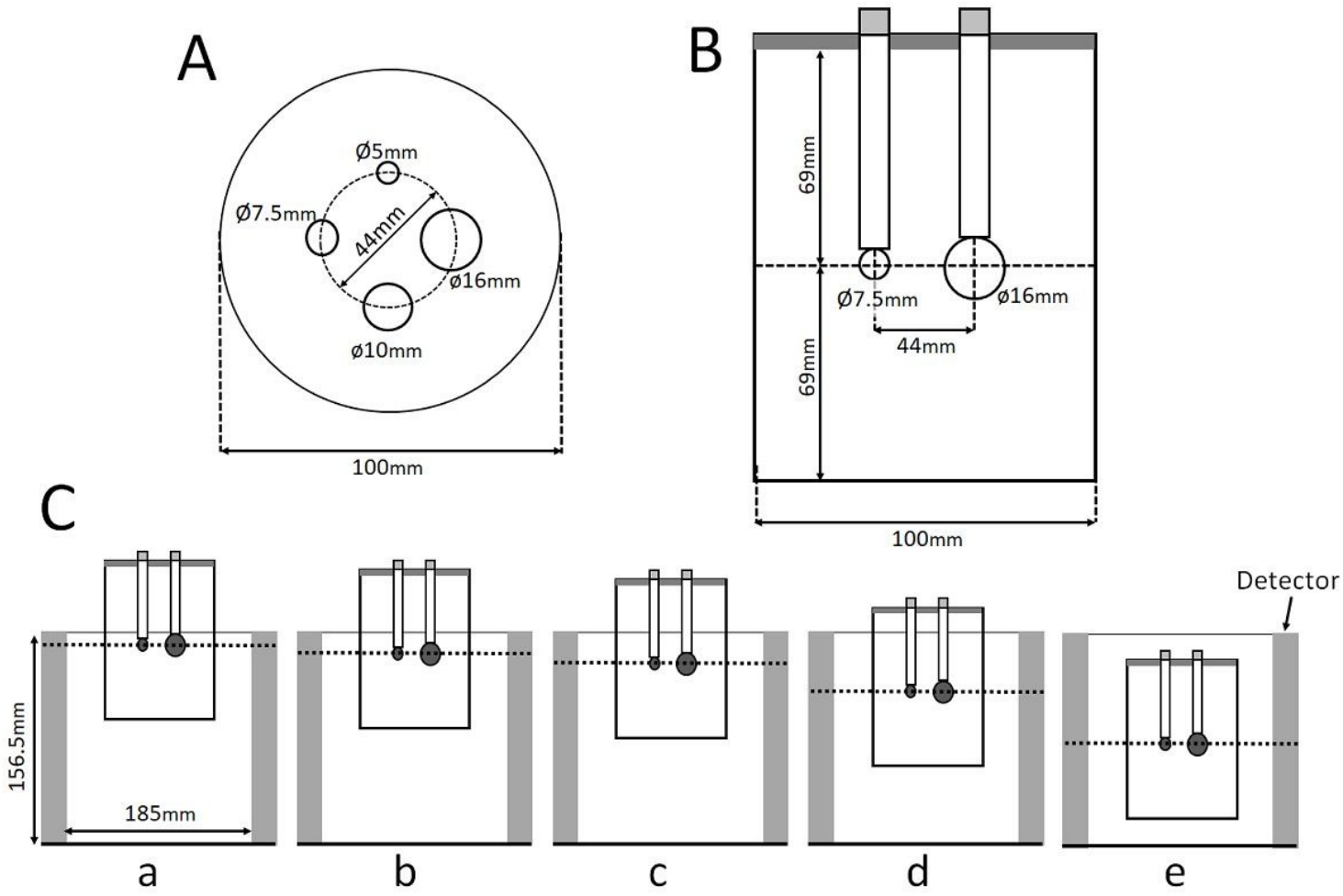

Figure 1

Cross-sections of the NEMA image quality phantom with dimensions. An axial plane view (A) and a lateral view (B) of the breast phantom in which the spheres were arranged. (C) Relationship between the detector and the phantom (lateral views). The distances from the upper edge of the detector were 8 mm (a), 13 mm (b), 19.5 mm (c, depth of 1/8), 39.5 mm (d, depth of 1/4), and 78 mm (e, depth of 1/2, the centre of the detector)

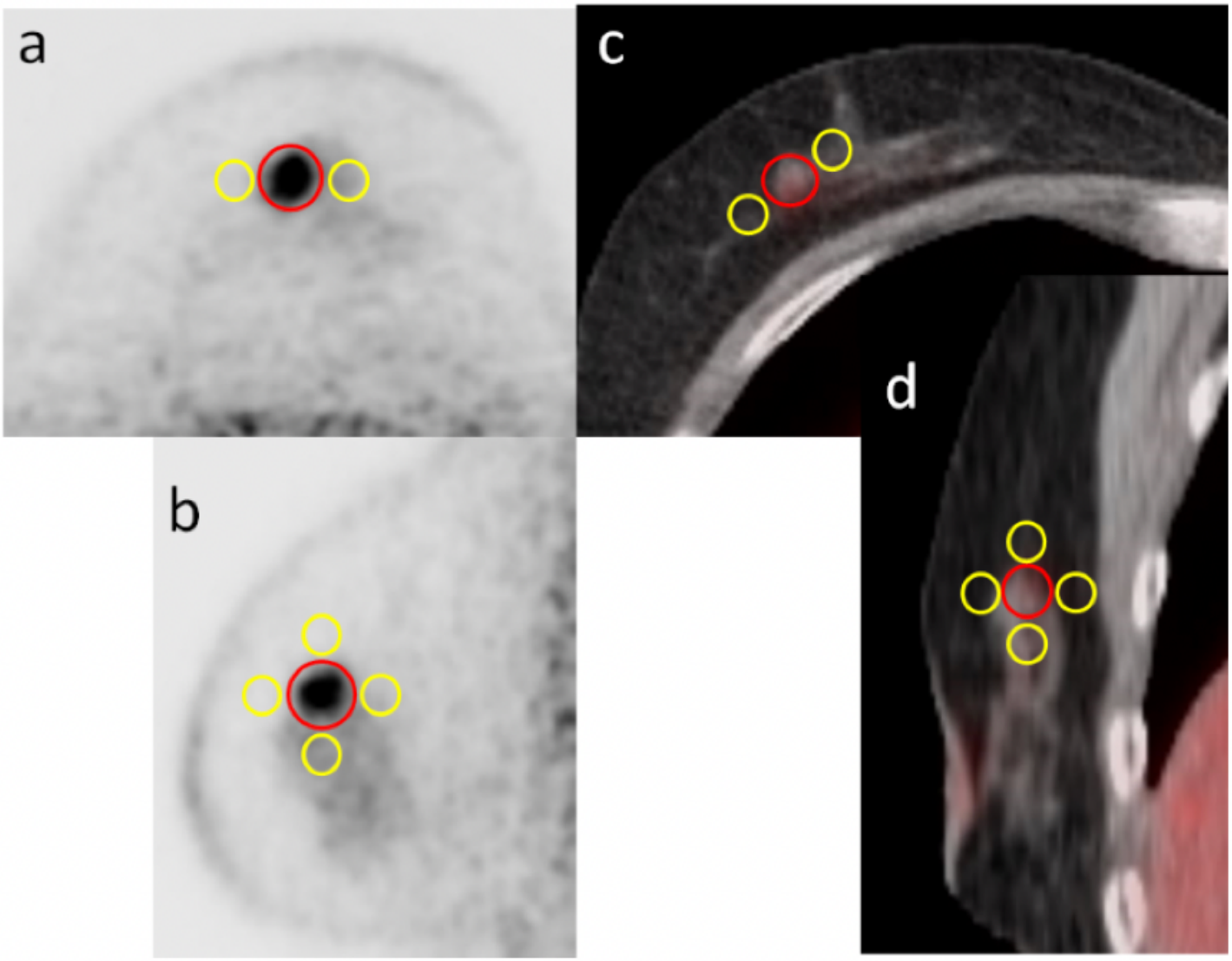

Figure 2

Positioning of the volume of interest (VOI) for the measurement of clinical PET images. A spheroid VOI (red) on FDG uptake of the tumour and 5 (or 6) spherical VOIs (yellow) were placed to calculate the TBR. Transaxial and sagittal images of dbPET (a, b) and whole-body PET/CT (c, d)

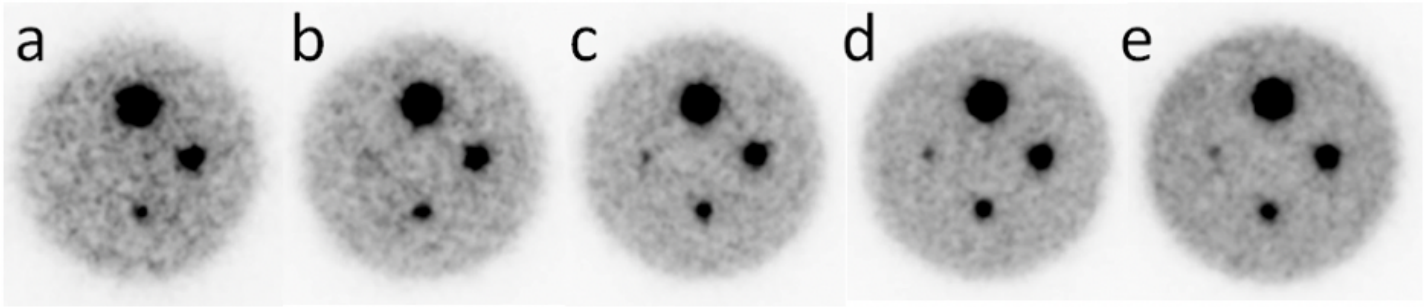

Figure 3

Images of the breast phantom scanned by dbPET at the five different positions. Images a, b, c, d, and e correspond to phantom images scanned at 8 mm, 13 mm, 19.5 mm (depth of 1/8), 39 mm (depth of 1/4), and 78 mm (depth of 1/2, the centre of the detector) below the top edge of the detector. Closer to the edge of the detector, the background was noisier. The hot spots of the smallest sphere with a diameter of 5 mm could not be confirmed in a and b. dbPET, dedicated breast positron emission tomography

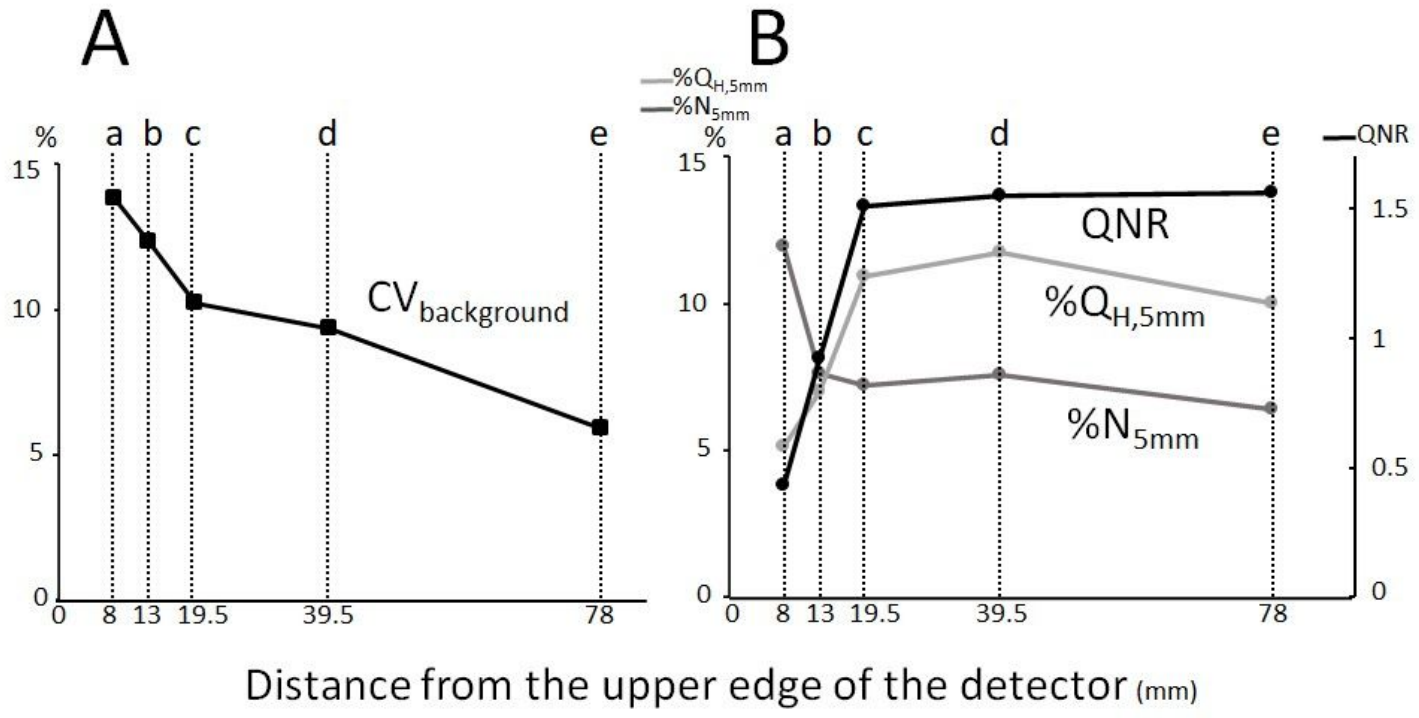

Figure 4

Quantitative assessment of the breast phantom scanned by dbPET at the five different positions. Line graphs of CVbackground (A), %QH,5mm, %N5mm, and QNR (B) of the breast phantom images scanned by dbPET at the five different positions are shown. The a, b, c, d, and e on the X axis correspond to phantom positions of 8 mm, 13 mm, 19.5 mm (depth of 1/8), 39 mm (depth of 1/4), and 78 mm (depth of 1/2, the centre of the detector) below the top edge of the detector. CVbackground, coefficient of variation of the background; dbPET, dedicated breast positron emission tomography; %QH,5mm, percentage of the contrast; %N5mm, percentage of background variability; QNR, %QH,5mm-%N5mm-ratio.

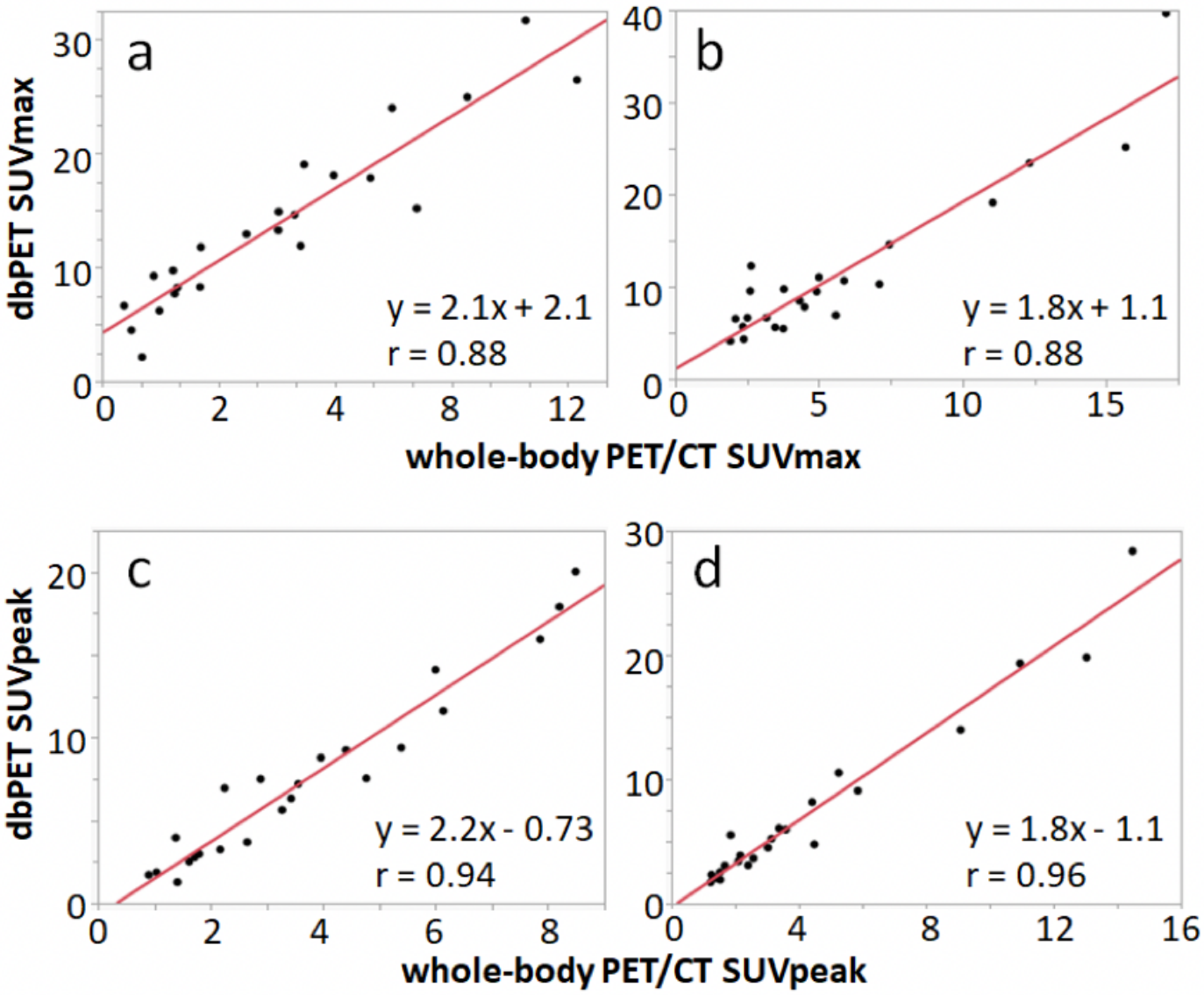

Figure 5

Correlation of quantitative parameters between dbPET and whole-body PET/CT. The graphs show the correlation of SUVmax and SUVpeak of dbPET with those of whole-body PET/CT in the peripheral group (a, c) and the non-peripheral group (b, d). In both peripheral and non-peripheral groups, the SUVmax and SUVpeak of dbPET were higher than those of PET/CT with high correlation

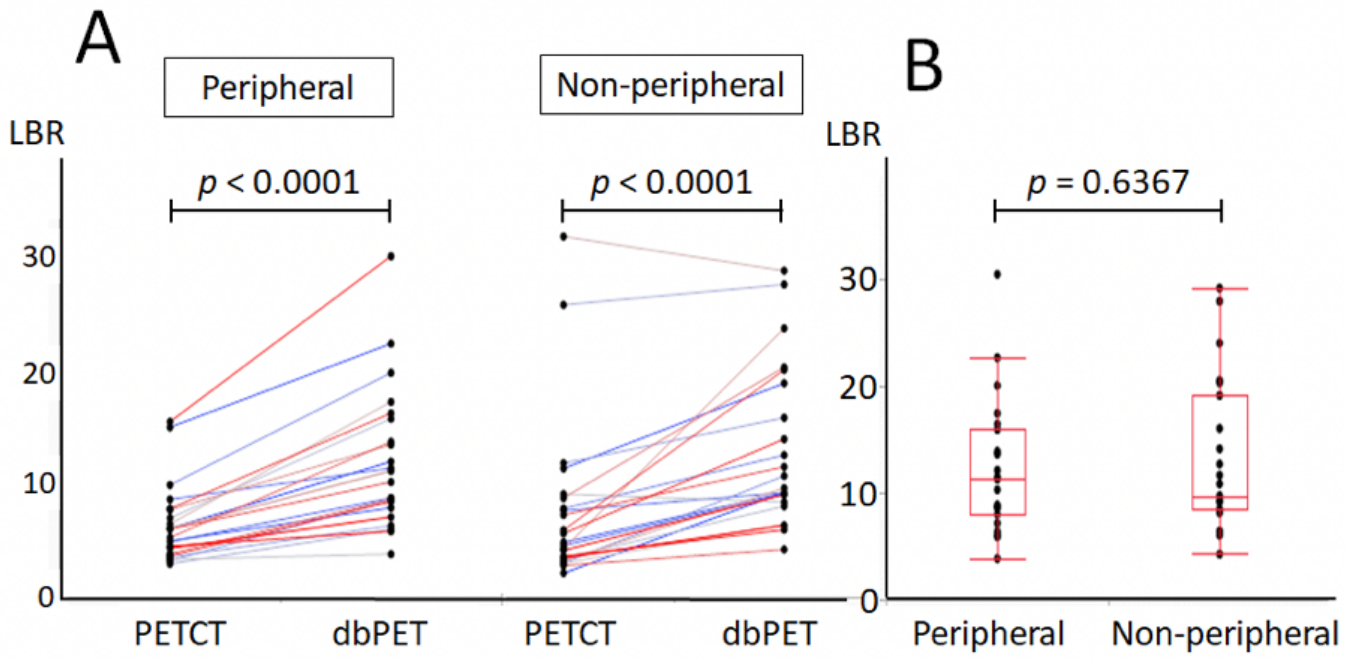

Figure 6

Comparisons of tumour-to-background ratios (TBRs). There were significant differences between TBRs of dbPET and whole-body PET/CT in both peripheral (p<0.0001) and non-peripheral (p<0.0001) groups (a). There was no significant difference in the TBR of dbPET between the peripheral and non-peripheral groups (p=0.6367, b)

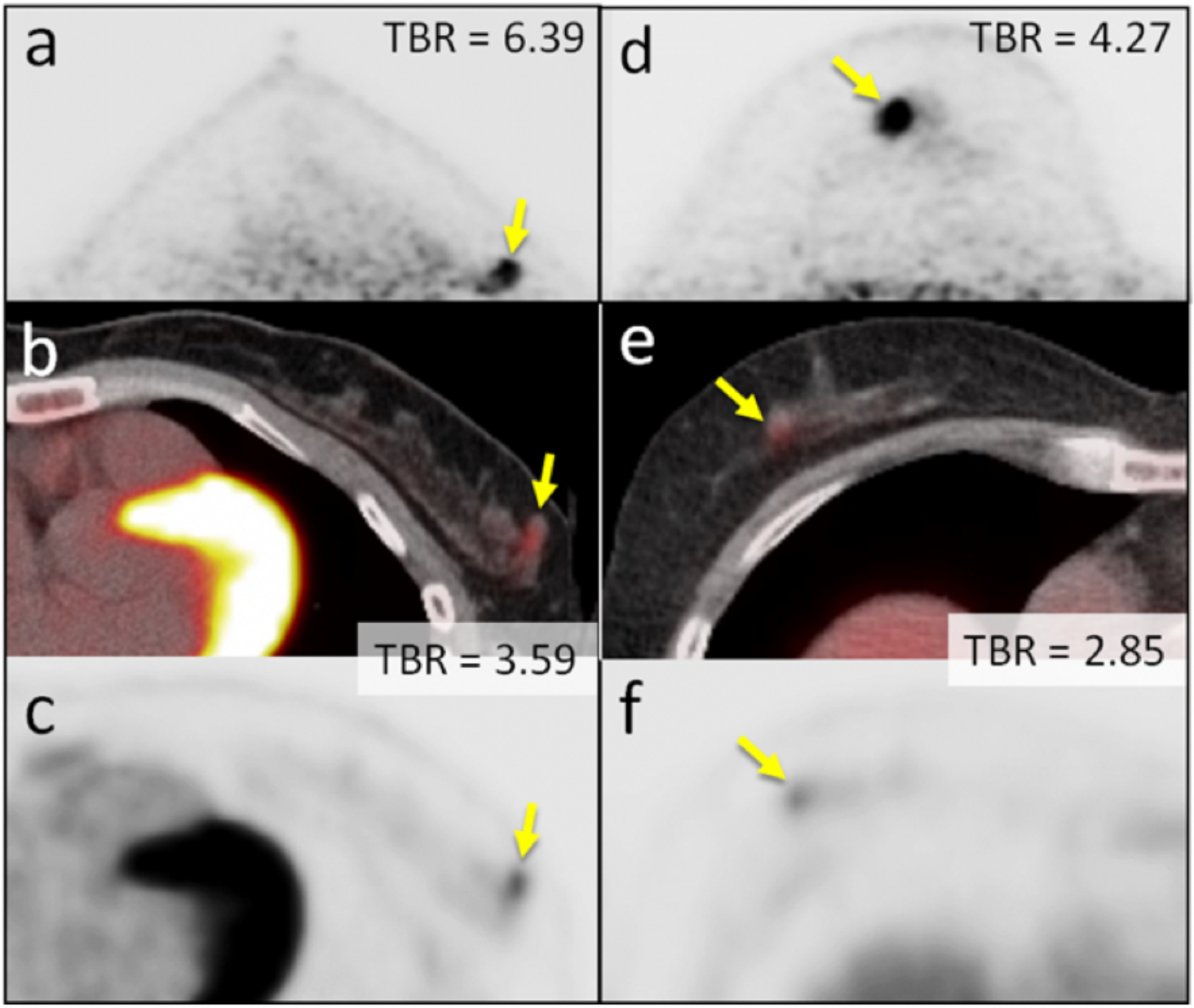

Figure 7

Peripheral and non-peripheral breast cancer images of dbPET and whole-body PET/CT. Representative clinical images of peripheral (39-year-old woman; clinical size, 12 mm; a, b, and c) and non-peripheral (63-year-old woman; clinical size, 9 mm; d, e, and f) breast cancers on dbPET (a, d), PET/CT (b, e), and PET (c, f) with focal FDG uptake in the background mammary gland tissue. Although the focal uptakes were visualised on both the dbPET and whole-body PET/CT images, it was obvious on dbPET with higher TBR than that on whole-body PET/CT, regardless of the peripheral or non-peripheral location.

Supplementary Files

This is a list of supplementary files associated with this preprint. Click to download.

- formulas.docx